Springer

Journal of
Mechanical
Science and
Technology

Journal of Mechanical Science and Technology 22 (2008) 895~904

www.springerlink.com/content/1738-494x

Design, drive and control of a novel SMA-actuated humanoid flexible gripper

Kai Yang* and Yanjue Wang

College of Electrical and Electronic Engineering, Huazhong University of Science and Technology, Wuhan, People's Republic of China

(Manuscript Received July 16, 2007; Revised February 15, 2008; Accepted February 23, 2008)

Abstract

An elemental SMA actuator, consisting of an elastic rod with two embedded SMA wires, is presented. The recovering wire w_1, with remembered 'U' shape, is located along the rod's axis. The restoring wire w_2, with memorized straight shape, is located in parallel with the rod' axis with an offset distance d_1. Two strain gauges, arranged in complemental configuration and sticking to the rod, are used to implement accurate displacement control. Upon the elicitation of the structure of a human being's hands, a finger with multi-units is proposed. The finger has two flexible rods with embedded SMA wires and one shorter rod as a connecting part. The number and position of fingers are investigated by making use of a nonlinear plan process with an index W, a function of grasp matrix G. The hardware of the drive and control system of the gripper has been completed on the base of a DSP chip. After the track plan is realized in the joint space through B spline interpolation method, the software of the position control system is fulfilled through two-staged slide control strategy. The simulations and experiments of step response of the SMA actuator are carried out. It is shown in the experiments that the maximum angle between ends' tangents of each finger is 68.5, 79 and 79 degrees, respectively, and the tip of each finger could reach its final position by using approximately the same time period.

Keywords: SMA-actuated; Flexible; Gripper, Design; Drive and control

1. Introduction

Several unique and fascinating multi-degree-of – freedom grippers have been developed over the past twenty years, primarily using traditional means of actuation [1-4]. Though there are many grippers, there are only a few using a new approach to classical gripper power. These grippers that utilize advanced or smart actuators are listed below. The Hitachi Ltd. Gripper uses SMA wires. This four-fingered gripper weighs 9.9lbs. and is 27.5inches long. Possible applications for this gripper include maintenance work in hostile environments, medical micro-manipulators, and undersea operations [5]. Two other SMA actuated grippers are a biomechanic gripper and a Fingerspelling Gripper. The biomechanic gripper is a five-fingered gripper utilizing four Flexinol NiTi wires per finger, which are connected on the upper and lower part of the finger's body on both sides [6]. The Fingerspelling Gripper presents data from a computer one character at a time using a finger-spelling alphabet, which is read by the user placing the gripper on the device. The gripper has a forearm attached that houses the 108, 250 micron Flexinol wires acting in parallel [7].

Though there has been much research accomplished on SMAs, there is still a need for new design methodologies and paradigms for lightweight, practical grippers for robotic systems. It is known that the advantages of conventional SMA actuators include their incredibly small size, volume and weight; their high force to weight ratio and their low cost [8-10]. Their limitations include complex structure, band-

*Corresponding author. Tel.: +86 27 875 43428, Fax.: +86 27 875 43428
E-mail address: kkyhust@163.com
DOI 10.1007/s12206-008-0215-1

width and efficiency restrictions, cartoon and discontinuous movements, limited life cycle and non-linear effects such as hysteresis phenomena. It is proposed that the novel design methodology and prototype fabrication discussed in this paper will aid in the advancement and the development of an embedded elemental SMA actuator for Humanoid Flexible Gripper. The design, drive and control of the gripper are discussed in detail.

2. Design and fabrication

2.1 Elemental SMA actuator

Fig. 1 shows the elemental SMA actuator prototype's structure. The two SMA wires, with the same radius r_s, are embedded in an elastic rod, with the radius R_r. The recovering wire w_1, with remembered 'U' shape, in other words, bending upon being heated to suitable temperature, is located along the rod's axis. On the other hand, the restoring wire w_2, whose remember shape is straight, in other words, returning to beeline upon being heated to certain temperature, is located in parallel with the rod's axis with an offset distance d_1. To realize precise displacement control, a curvature sensor with two strain gauges is designed. As shown in the figure, the two strain gauges, denoted by G_1 and G_2, are arranged in complemental configuration. With a dimension 3mm in width and 5mm in length, the gauges stick to the center of the rod's outside surface making use of 502glue. When the actuator is actuated, the resistance varieties of two gauges have the same values. The final curvature's signal can be derived by a half measuring bridge cooperating with the resistance varieties.

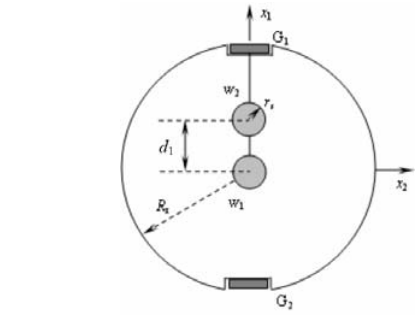

(a) Cross section

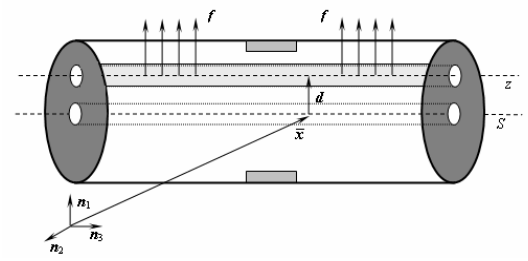

(b) Side view

Fig. 1. Sketch diagram of planar bending ESMAA.

If wire w_1 is heated by suitable current, the wire recovers to 'U' shape upon the temperature above A_s (the austenite phase transformation beginning temperature). The rod will bend subsequently. When stopping heating wire w_1 and heating wire w_2 by suitable current instead, the restoring force of the wire causes the rod return to default straight immediately. So, the actuator possesses the ability to move in two directions and the movement is smooth, flexible and fast.

As shown in Fig. 1, the vector form of the equations of equilibrium of a flexible rod acted upon by a distributed force, $\boldsymbol{f}$, acting at a distance $\boldsymbol{d}$ from the centroid, is [11, 12]

$$\frac{\mathrm{d}\boldsymbol{F}}{\mathrm{d}S} + \boldsymbol{f} = 0 \tag{1}$$

$$\frac{\mathrm{d}\boldsymbol{M}}{\mathrm{d}S} + \frac{\mathrm{d}\bar{\boldsymbol{x}}}{\mathrm{d}S} \times \boldsymbol{F} + \boldsymbol{m} = 0 \tag{2}$$

where $\boldsymbol{F}$ is the rod resultant force vector and $\boldsymbol{M}$ is the rod resultant moment vector, S denote the arc length along c and $\boldsymbol{m}$ denotes moment from SMA wire to the rod. Considering the situation that wire w_2 is heated, if k_2' is the recoverable curvature of wire w_2 and F^a is the recovering force, the moment M_2 is obtained as

$$M_2 = (1 - d_1 k_2) k_2' E^a I^a \tag{3}$$

where M_2 is the component moment of the rod, k_2 is the actual curvature of the rod, and E^a, I^a are Young's moduli and moment of inertia of the cross-section of the wire, respectively. Since the following constitutive assumption is made using beam theory

$$M_2 = EIk_2 \tag{4}$$

where E, I are Young's moduli and moment of the cross-section of the rod, respectively. Then, the actual curvature is

$$k_2 = \frac{k_2' E^a I^a}{EI + d_1 k_2' E^a I^a} \tag{5}$$

While wire w_1 is heated then d=0 and m_2=0. Simi-

larly, the curvature of the rod is

$$k_2 = \frac{k_1' E^a I^a}{EI} \tag{6}$$

Accordingly, the actuator's curvature is obtained by making use of Eqs. (5) and (6):

$$k_2 = \begin{cases} \dfrac{k_1' E^a I^a}{EI} & w_1 \text{ is heated} \\ \dfrac{k_2' E^a I^a}{EI + d_1 k_2' E^a I^a} & w_2 \text{ is heated} \end{cases} \tag{7}$$

2.2 Humanoid gripper

Since the elemental SMA actuator has the ability to move in a set direction and output force steadily, it is used to build a humanoid flexible gripper. In order to increase the bending angle of the finger and to realize smoothly an anthropomorphic grasping, upon the elicitation of the structure of the human being's hands, a novel robot finger with multi-units is proposed, as shown in Fig. 2. The finger has two flexible rods with embedded SMA wires and one shorter rod as a connecting part.

The structure of the SMA-actuated gripper is determined according to that of the human hand. To validate the elementary principle, the number and position of fingers should be ascertained firstly. The least number of fingers for a steady grasp is three. Besides, there is no sense that the number is more than five. Otherwise, more fingers will result in a more complex control system. From the investigation on the manipulation of the human hand, one can conclude that almost all grasps could be completed by three fingers. Finally, the number of fingers is set as three. The next step is to determine the location of the fingers. To begin with, the grasp plan is carried out with the goal of finding the best contact points within the object's feasible operation range, i.e., the grasp that has the best stability. The process is described as the following nonlinear plan problem:

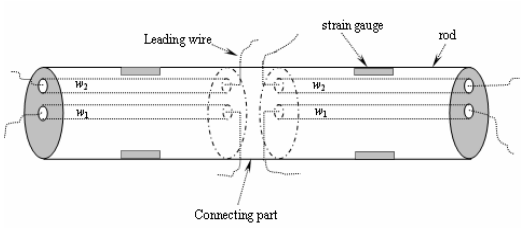

Fig. 2. Schematic diagram of the finger.

$$\begin{cases} \min(-W) = \min(-\sqrt{\det(\boldsymbol{G}\boldsymbol{G}^{\mathrm{T}})}) \\ \{(x_i, y_i, z_i) \mid S(x, y, z) = 0 \text{ , } i = 1, 2, \cdots, m\} \\ (x_i, y_i, z_i) \in g(x, y, z) \text{ , } i = 1, 2, \cdots, m \end{cases} \tag{8}$$

where x_i, y_i and z_i denote the coordinates of the i^{th} contact point, $S(x, y, z) = 0$ depicts the equation of the operated object's profile, $g(x, y, z)$ represents the feasible operation range, W is the plan index, and G is the grasp matrix.

In general, the grasp matrix is expressed as:

$$\boldsymbol{G} = \begin{bmatrix} \boldsymbol{I} & \boldsymbol{I} & \cdots & \boldsymbol{I} \\ \boldsymbol{R}_1 & \boldsymbol{R}_2 & \cdots & \boldsymbol{R}_m \end{bmatrix} = \begin{bmatrix} \bar{\boldsymbol{I}} \\ \bar{\boldsymbol{R}} \end{bmatrix},$$

where $\bar{\boldsymbol{I}} \in \boldsymbol{R}^{3\times 3m}$, $\bar{\boldsymbol{R}} \in \boldsymbol{R}^{3\times 3m}$, m is the number of contact points and

$$\boldsymbol{R}_i = \begin{bmatrix} 0 & -z_i' & y_i' \\ z_i' & 0 & -x_i' \\ -y_i' & x_i' & 0 \end{bmatrix},$$

where $(x_i\ y_i\ z_i)$ is the coordinates of the i contact point in the body reference frame.

The grasp analysis of the three-fingered gripper is

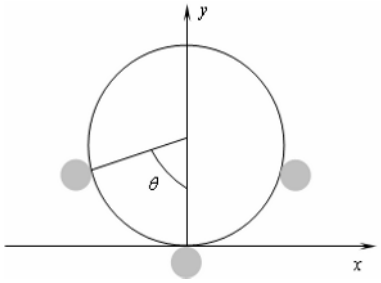

Fig. 3. Displacement relation between three contact points.

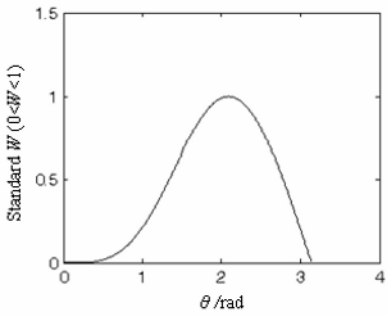

Fig. 4. Relation between index W and θ .

completed making use of the index W. Consider a sphere with the radius 20mm. The location of the first finger is fixed and the location of the other two fingers is described by θ, as shown in Fig. 3. Fig. 4 is the relation between index W and θ. When $\theta = \pm 2\pi/3$, W reaches its maximum, which means the best stability. On the basis of the analysis, three fingers arrange at the vertexes of an equilateral triangle equally.

3. Drive and control

3.1 Drive and measurement

The operation of SMAA depends on the phase transformation of SMA wire, which is realized by temperature cycles. The drive and control system consists of the DSP miniature system, drive module and measure module. The DSP miniature system consists of the core CPU, clock and reset circuit and extended external memory. The drive module consists of wave generator, signal amplifier and power drive. The measure module consists of electrical bridge, signal amplifier and filter. The system diagram is as follows.

The DSP chip TMS320LF2407 is chosen to develop the minimum system. To meet the requirement of debugging, an external 10 MHz oscillator and two 64K×16 bit high speed SRAM, IC61LV6416-10T, are needed, as shown in Fig. 6.

The PWM technique, modifying the duty ratio of the heat current, is found to be the best drive manner. To begin with, the signal of the sensors is measured to be compared with the set value. Then, the next heat pulse width is calculated by the means of suitable control arithmetic. There are at least two advantages for the drive manner mentioned above. One is that, thanks to the integration of heat current, the gripper would never output incontinuous movement. The other is that the digital signal could be controlled easily without a D/A converter. As shown in Fig.7, a square wave with adjustable width goes out through the affair manager. Since the high electrical level of the signal falls in the range from zero to five voltages, which is not high enough to guarantee the open and close of the MOSFET, a level conversion chip, CD40109, is needed. The final signal then goes into the integrated chip TPS2812 to drive the MOSFET.

To realize precise displacement control, a curvature sensor with two strain gauges is designed, as shown in the figure. With a dimension of 3mm in width and 5mm in length, the gauges stick to the center of the rod's outside surface with use of 502glue. When the actuator is actuated, the resistance varieties of two gauges have the same values. The final curvature's signal can be derived by a half measuring bridge in cooperating with the amplifier, as shown in Fig. 8.

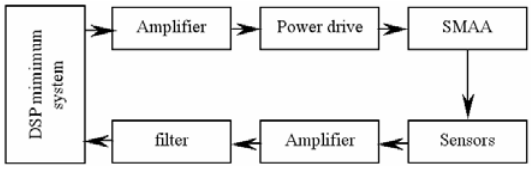

Fig. 5. Block diagram for drive and control system.

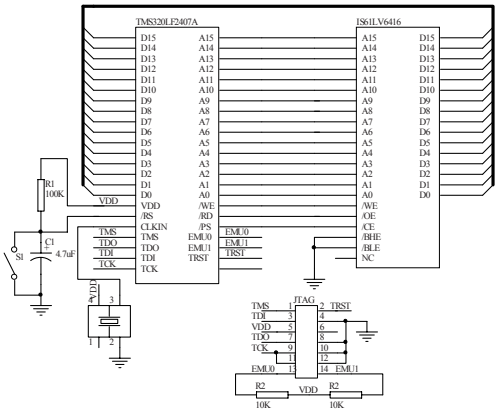

Fig. 6. Minimum system of DSP.

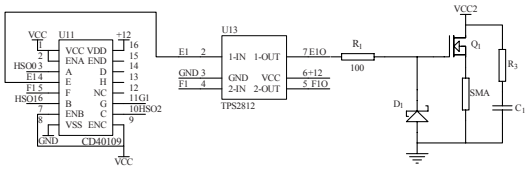

Fig. 7. Drive module.

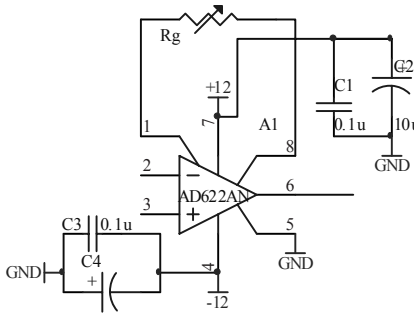

Fig. 8. Amplifying Circuit using AD622.

3.2 Track plan

On the base of robotics, the position relation between two ends of one finger is shown in Fig. 9. One end is set as the original point and the other one can move freely. The angle between tangents of ends is denoted as θ, l_1 and l_3 are lengths of leading and following knuckles, respectively, and l_2 represents the length of the connecting part. The movement equation of the finger, i.e., transformation matrix between two ends, is expressed as

$$T=\begin{bmatrix}\cos\theta & \sin\theta & 0 & x_e\\ \sin\theta & \cos\theta & 0 & y_e\\ 0 & 0 & 1 & 0\\ 0 & 0 & 0 & 1\end{bmatrix} \tag{9}$$

Since the track plan in the joint space has advantages such as directly using the controllable variables, real time execution and easy to approach, it's used in our work. The steps are as follows: ① According to several set points on the track of finger-tip, the angles θ_1 θ_3 for each points are derived from Eq. (1). Consequently, each middle point can be regarded as either the start point or finish point, and at those points the speed is not zero. ② The track of each knuckle is created through relevant arithmetic. The conventional arithmetic consists of cube polynomial interpolation, parabola transition linear interpolation and B spline interpolation [13, 14]. Among them, B spline interpolation is the most simple, convenient to modify and strictly coincident with all crunodes. Besides, using the method, not only the crunode's position but also its reciprocal, i.e., velocity, is also continuous. Let the nodes list P_1, P_2, P_3, …, P_n be approached by curves list C_1, C_2, C_3, …, C_{n-1}.

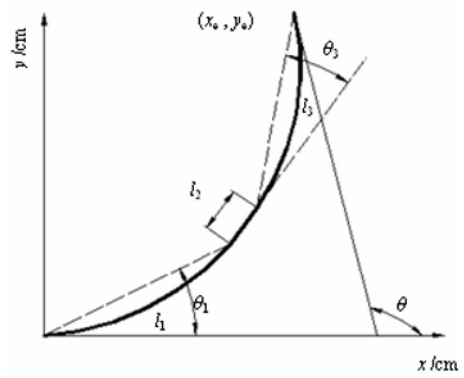

Fig. 9. Position relation between two ends of finger.

Each curve is controlled by several nodes in the list and depicted as

$$\begin{aligned}C_i(u)&=[x(u)\quad y(u)\quad z(u)]\\&=\sum_{j=0}^{k}N_{j,k}(u)V_{i+j-1}\end{aligned} \tag{10}$$

Where i=1, 2…, n-1, k means degree, V_{i+j+1} denotes the control points and $N_{j,k}(u)$ is the basic function and defined as

$$N_{j,1}(u)=\begin{cases}1 & t_j\le u\le t_{j+1}\\ 0 & \text{other}\end{cases} \tag{11}$$

and

$$\begin{aligned}N_{j,k}(u)&=\frac{(u-t_j)N_{j,k-1}(u)}{t_{j+k-1}-t_j}+\\&\frac{(t_{j+k}-u)N_{j+1,k-1}(u)}{t_{j+k}-t_{j+1}}(t_{k-1}\le u\le t_{n+1})\end{aligned} \tag{12}$$

where t_j represents the crunode's value. If four crunodes are picked to build a B spline curve, the function matrix is denoted as

$$N_{i,3}(u)=\frac{1}{6}[u^3\quad u^2\quad u\quad 1]\begin{bmatrix}-1 & 3 & -3 & 1\\ 3 & -6 & 3 & 0\\ -3 & 0 & 3 & 0\\ 1 & 4 & 1 & 0\end{bmatrix} \tag{13}$$

then the conjoint two curves have the following expressions

$$\begin{aligned}C_{i,3}(u)&=N_{0,3}(u)V_{i-1}+N_{1,3}(u)V_i\\&+N_{2,3}(u)V_{i+1}+N_{3,3}(u)V_{i+2}\end{aligned} \tag{14}$$

$$\begin{aligned}C_{i+1,3}(u)&=N_{0,3}(u)V_i+N_{1,3}(u)V_{i+1}\\&+N_{2,3}(u)V_{i+2}+1+N_{3,3}(u)V_{i+3}\end{aligned} \tag{15}$$

Consequently, the i^{th} cube spline curve is depicted as

$$C_{i,3}(u)=\frac{1}{6}[u^3\quad u^2\quad u\quad 1]\begin{bmatrix}-1 & 3 & -3 & 1\\ 3 & -6 & 3 & 0\\ -3 & 0 & 3 & 0\\ 1 & 4 & 1 & 0\end{bmatrix}\begin{bmatrix}V_{i-1}\\ V_i\\ V_{i+1}\\ V_{i+2}\end{bmatrix} \tag{16}$$

where $u\in[0,1]$ and i = 1, 2, …, n-1. The relation between control points and crunodes is

Table 1. Coordinates of finger-tip at different crunodes.

Crunode	1	2	3	4	5
x (mm)	143	136	118	103	90
y (mm)	18.8	34.5	55.8	62.6	65.8

Table 2. Bending angles of knuckle at crunodes.

Crunode	1	2	3	4	5
θ_1 (rad)	0.2	0.5	0.9	1.3	1.54
θ_3 (rad)	0.2	0.35	0.64	0.78	1.03

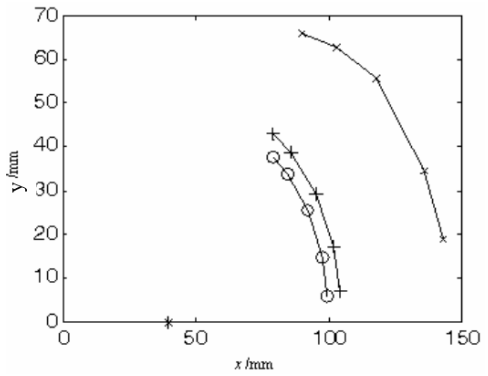

Fig. 10. Position of ends at crunodes.

$$C_{i-1,3}(1) = C_{i,3}(0) = P_i \quad (\mathrm{i} = 1,\ 2,\ \ldots,\ \mathrm{n}) \tag{17}$$

from Eq. (16)

$$C_{i-1,3}(1) = C_{i,3}(0) = (1/6)(V_{i-1} + 4V_i + V_{i+1}) \tag{18}$$

So, if the number of crunodes is n, the number of control points should be n+2. Obviously, the values of V_0 and V_{n+2} should be added. If the superposition boundary condition $V_0 = V_1$ and $V_{n+1} = V_n$ is adopted, the final relation between control points and crunodes is derived from Eqs. (17), (18).

$$\begin{bmatrix} 6 & -6 & & & & & \\ 1 & 4 & 1 & & & & \\ & 1 & 4 & 1 & & & \\ & & & \cdots & & & \\ & & & & 1 & 4 & 1 \\ & & & & & 6 & -6 \end{bmatrix} \begin{bmatrix} V_0 \\ V_1 \\ V_2 \\ \cdots \\ V_n \\ V_{n+1} \end{bmatrix} = \begin{bmatrix} 0 \\ P_1 \\ P_2 \\ \cdots \\ P_n \\ 0 \end{bmatrix} \tag{19}$$

Subsequently, several crunodes of finger-tip are determined; five points in table 1 and the corresponding knuckle bending angles are shown in Table 2. The position for the ends and the track of two joint variables, i.e., bending angles, are represented in Fig. 10 and Fig. 11 respectively.

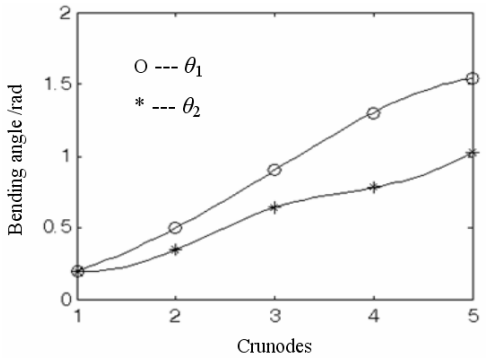

Fig. 11. Track plan of bending angles of ESMAA.

3.3 Displacement control

Due to the nature of the shape-memory effect, the SMAA is inherently a non-linear device exhibiting significant hysteresis in the strain-temperature, stress-strain and resistance-temperature relations. So, a nonlinear variable structure control strategy is adopted [15-17]. The key point of the control system lies in the switching function and control law so as to make the whole closed loop system meet the following restrictions: ① The sliding mode does exist; ② The range of sliding mode is large enough to make the state trajectory, starting from any initial conditions, and is driven towards the switching surface ; ③ The sliding mode is steady gradually. The condition (c) is guaranteed by proper switching function, s. Combined with control law, the switching function s is

$$s = e \tag{20}$$

and the switching surface is

$$s = e = 0 \tag{21}$$

where e is the actuator's curvature error.

The duty ratio of heat current is

$$d_{\mathrm{r}} = \begin{cases} d_{\mathrm{high}} & e > 0 \\ 0 & e < 0 \end{cases} \tag{22}$$

In the period of heating the wires, the time constant is small so that the model is simplified as an integrator; then

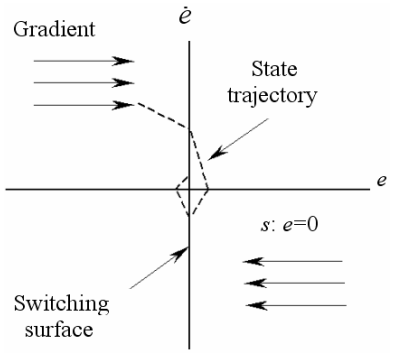

Fig. 12. Phase diagram of error.

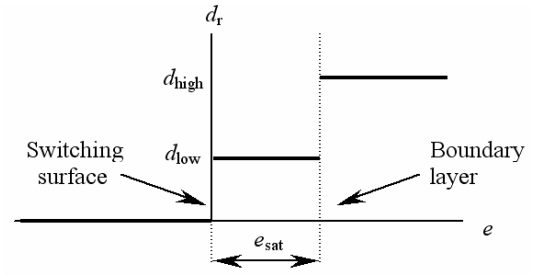

Fig. 13. Two-staged slide mode controller.

$$x = x_0 + \int_0^t K * d_r \mathrm{d}t \tag{23}$$

$$\dot{e} = -\dot{x} = -K * d_r \tag{24}$$

where x_0 denotes the set curvature, x is the actual curvature and K is the gain. To ensure that the state trajectory in the error phase diagram is driven towards the switching surface, we could get

$$\mathrm{sgn}(d_r) = \mathrm{sgn}(e) \tag{25}$$

through the sliding mode existence condition

$$s \cdot \dot{s} < 0 \tag{26}$$

where the error is positive, the curvature is less than the set value and the controller outputs current pulse with certain duty ratio to heat the SMA wires. However, when the error is negative, the duty ratio is zero and the SMA wire begins to cool down. Any perturbations from the switching surface result in an immediate control signal that forces the trajectory back onto the switching surface, and the gradient of the state space vector is always vertical to the switching surface, as shown in Fig. 12. In the time optimal sense, switching is the most efficient way to drive the plant since the maximum realizable gain is used. To maintain the stability of the system, the gain d_{high} must be

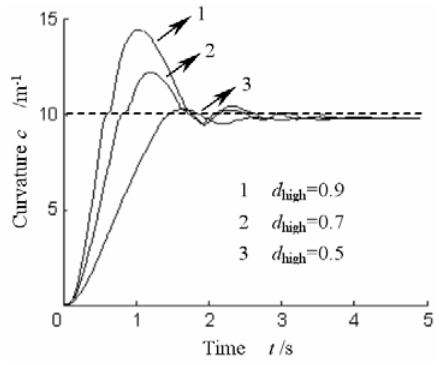

Fig. 14. Two-staged control of different d_{high}.

chosen so that it is large enough to drive the plant as quickly as required to the set point, yet be small enough so as to not cause oscillation larger than a specified limit.

Since using a single gain in the feedback path results in a controller that is too conservative, a two-staged controller has been explored for the control of the SMA actuator. If the error is large, then the maximum constant feedback k_{high} is used. As the state trajectory approaches the boundary layer the control is switched to low gain k_{low}. This results in a smoother motion as the state trajectory slows down as it approaches the set point switching surface. The block diagram of the controller can be seen in Fig. 13.

In the controller design, d_{low} should be determined carefully. If the SMA wire's temperature is T_{set} as the curvature of the actuator arrives at the set point and the duty ratio of the heat current is d', the d_{low} should be equal to d' so as to keep the actuator in heat balance and the temperature of wire stay at T_{set}.

4. Simulation and experiments

4.1 Simulated results

The simulated results show that control parameters have a sharp influence on the controller characteristics; as indicated in Figs.14-16, the control inputs are indicated by the dotted lines. When d_{high} decreases, the overshoot decreases, rise time increases and the response slows down subsequently. When d_{low} decreases, the steady error decreases slightly. When e_{sat} decreases, the overshoot increases accordingly.

Fig. 17 shows the step response result with the control parameters d_{high} = 0.5, d_{low} = 0.2, e_{sat} = 0.2; the target curvature is 10m^{-1} and sampling time is 0.05s. From the simulated curve, the rise time is 1.2s, over

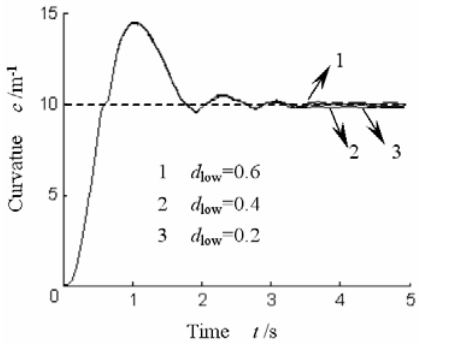

Fig. 15. Two-staged control of different d_{low}.

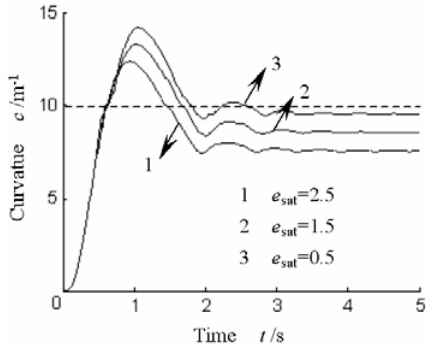

Fig. 16. Two-staged control of different e_{sat}.

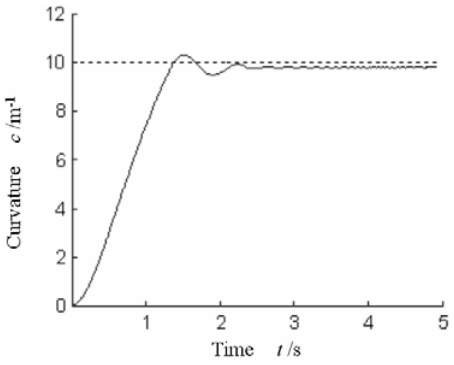

Fig. 17. Step response of two-staged slide mode control.

shoot is 2% and steady error is 0.2m^{-1}. The control signal is found to be discontinuous and the steady response trajectory enters limit cycles with the frequency 160Hz and maximum magnitude 0.03m^{-1}, i.e., high frequent periodical oscillation, as shown in Fig. 18. As a matter of fact, the oscillations have slight influence on the stability of the controller. Finally, the principle to determine the control parameters is derived from the simulation: ① If the transition time is long, then decrease d_{high}; ② If the overshoot is too big

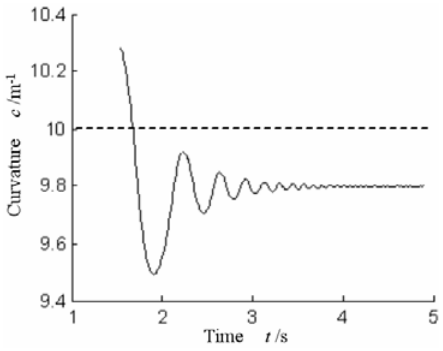

Fig. 18. Oscillation of the controller.

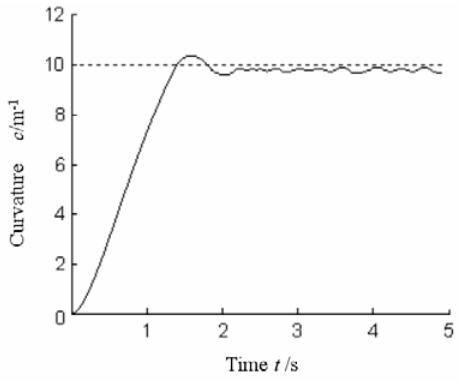

Fig. 19. Experimental result of step response using two-staged slide mode control.

and rise time is too short, then decrease d_{high}; ③ If the target curvature increases, then increase d_{low}; ④ If the maximum magnitude of limit cycle is too big, then decrease d_{high}; ⑤ If the steady error is big, then decrease e_{sat}.

4.2 Experimental results

Fig. 19 shows experimental step response with the control parameters d_{high}=0.5, d_{low}=0.2, e_{sat}=0.2 and sampling time T = 54.7ms; the curvature is measured with sensors. It is obvious that the experimental result is similar to the simulation: the rise time is 1.21s, the overshoot is 2.5% and the steady error is 0.25m^{-1}. The controller is robust to parameters' variety.

Fig. 20 shows the step response of the PI controller with the parameters K_P = 0.06, K_I = 0.0045 and sampling time T = 54.7ms. It is found that the rise time is 1.6s, overshoot is 23.5% and steady error is 0.23. Near the steady portion, some anomalistic oscillations appear and the set point could not be tailed well. The purpose of controller should be guaranteed by adjust

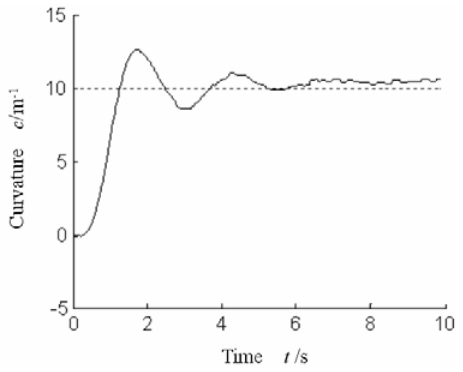

Fig. 20. Experimental result of step response using PI control.

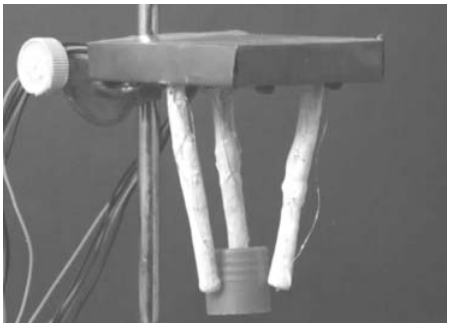

Fig. 21. Pictures of humanoid gripper.

ing K_P and K_I on-line so as to add difficulty to the control system. Consequently, the two-staged sliding mode controller is more simple and effective and becomes the ideal strategy for the SMAA. The disadvantage of this two-staged controller is that in the vicinity of the set point the feedback signal is low, so the plant is easily disturbed by perturbations. The further work is to justify the controller to be better robust against the perturbations while firmly maintaining the stability.

During operation, the grasp and fine manipulation are executed by the cooperation of three fingers. By the provision of joule heat obtained from a special supply, the temperature of the SMA wire reaches the transformation temperature easily, resulting in the anthropomorphic and flexible motion of the novel gripper. Once heating of the SMA wire is stopped, the gripper returns to its initial relaxed shape as soon as the temperature of the SMA wire drops.

Fig. 21 shows that the humanoid gripper was bent and returned to the default position when the currents were applied to some of the SMA wires. It is shown in the experiments that maximum angle between ends' tangents of each finger are 68.5, 79 and 79 degrees, respectively. The tip of each finger could reach its final position by using the same approximate time period, and by controlling the bending of each finger, the gripper could accomplish fine manipulation like that of a human being.

Since large current ability is required here, we chose a supply source with maximum voltage of 20 volts and maximum current of 20 amps. By strictly following manufacturing techniques, it is impossible for the specification of each finger to be the same completely; as a result, the simultaneity of movement cannot be met well. This is perhaps solved by improving the manufacturing process and choosing a special control strategy in future.

5. Conclusion

An elemental SMA actuator prototype's structure is presented, which consists of an elastic rod with two embedded SMA wires. The recovering wire w_1, with remembered 'U' shape, is located along the rod's axis. The restoring wire w_2 with memorized straight shape is located parallel to the rod's axis with an offset distance d_1. Two strain gauges, arranged in complemental configuration and sticking to the rod, are used to implement accurate displacement control. It is shown in the experiments that the actuator possesses the ability to move in two directions and the movement is smooth, flexible and fast.

Upon the elicitation of the structure of the human hand, a novel robot finger with multi-units is proposed. The finger has two flexible rods with embedded SMA wires and one shorter rod as a connecting part. From the investigation on the manipulation of the human hand, the number and position of fingers was ascertained by making use of a nonlinear plan process with an index W, a function of grasp matrix G. On the basis of the analysis, three fingers are arranged at the vertexes of an equilateral triangle equably.

The hardware of the drive and control system of the gripper has been completed on the base of a DSP chip. After the track plan is realized in the joint space through B spline interpolation method, the software of the position control system is fulfilled through a two- stage slide control strategy. The simulations and experiments of the step response of the SMA actuator are carried out. The results show that the humanoid gripper is bent and returns to the default position when a current are applied to some of the SMA wires.

It is shown in the experiments that maximum angle between ends' tangents of each finger are 68.5, 79 and 79 degrees, respectively. The tip of each finger could reach its final position by using approximately the same time period.

References

[1] M. J. Farrugia and M. A. Saliba, Optimisation of anthropomorphic robot hand design through human manual dexterity testing. *VDI Berichte*, 2006 (1956):147-152.

[2] R. Cabas, L. M. Cabas and C. Balaguer, Optimized design of the underactuated robotic hand. *ICRA* (2006) 982-987.

[3] S. Roccella, M. C. Carrozza and G. Cappiello, Design, fabrication and preliminary results of a novel anthropomorphic hand for humanoid robotics: RCH-1. *IEEE/RSJ International Conference on Intelligent Robots and Systems (IROS)*, (1) (2004) 266-271.

[4] M. S. Erden, K. Leblebicioglu and U. Halici, Multi-agent system-based fuzzy controller design with genetic tuning for a mobile manipulator robot in the hand over task. *Journal of Intelligent and Robotic Systems: Theory and Applications*, 39 (3) (2004) 287-306.

[5] M. E. Rosheim, Robot Evolution: The Development of Anthrobotics. *New York: John Wiley & Sons, Inc.*, (1994).

[6] I. Mihalcz, E. I. Zudor, V. Csibi and P. Baranyi. A biomechanic robot hand using SMA. *Tenth World Con. on Theory of Mach. and Mechanisms, Oulu*, Finland, June (1999) 1835-1840.

[7] R. G. Gilbertson, Muscle Wires Project Book. *California: Mondo-tronics, Inc.,* (1994) Third ed.

[8] A. D. Johnson, V. Martynov and V. Gupta, Applications of shape memory alloys: Advantages. Disadvantages. and limitations. *Proceedings of SPIE - The International Society for Optical Engineering*, (4557) (2001) 341-351.

[9] S. B. Choi, Y. M. Han, J. H. Kim and C. C. Cheong, Force Tracking Control of a Flexible Gripper Featuring Shape Memory Alloy Actuators, *Mechatronics*, 11 (6) September (2001) 677-690.

[10] Y. M. Han, C. J. Park and S. B. Choi, End-Point Position Control of a Single-Link Arm Using Shape Memory Alloy Actuators, *Proceedings of the Institution of Mechanical Engineers Part C - Journal of Mechanical Engineering Science*, 217 (8) Aug. (2003) 871-882.

[11] D. C. Lagoudas and T. G. Tadjbakhsh, Active flexible rods with embedded SMA fibers. *Smart Mater.Struct*, (1) (1992) 162-167.

[12] B. J. D. Blonk and D. C. Lagoudas, Actuation of elastomeric rods with embedded two-way shape memory alloy actuators. *Smart mater.struct*, (7) (1998) 771-783.

[13] H. Park and J. H. Lee, B-spline curve fitting using dominant points. *Lecture Notes in Computer Science*, ICCS 2006 (3992) 362-366.

[14] N. Caglar and H. Caglar, B-spline solution of singular boundary value problems. *Applied Mathematics and Computation*, 182 (2) 1509-1513.

[15] S. V. Drakunov, B. Ashrafi and A. Rosiglioni, Yaw control algorithm via sliding mode control. *Proceedings of the American Control Conference*, (1) (2000) 580-583.

[16] A. Sosa, L. Jorge, M. Castilla et al., Sliding mode control for the fixed-frequency series resonant converter with asymmetrical clamped-mode modulation. *ISIE* (2005) 675-680.

[17] C. Edwards and S. K. Spurgeon, Sliding Mode Control Theory and Applications, *Taylor & Francis*, (1998).